COMBINED DERIVATIVE/ANTIDERIVATIVE ANTIALIASING

Martin Holters

Department of Signal Processing and Communication
Helmut Schmidt University – University of the Federal Armed Forces
Hamburg Germany
martin.holters@hsu-hh.de

ABSTRACT

Nonlinear systems play an important role in musical signal processing, but their digital implementation suffers from the occurrence of aliasing distortion. Consequently, various aliasing reduction methods have been proposed in the literature. In this work, a novel approach is examined that uses samples of a signal's derivative in addition to the signal's samples themselves. This allows some aliasing reduction, but is usually insufficient on its own. However, it can elegantly and fruitfully be combined with antiderivative antialiasing to obtain an effective method. Unfortunately, it still compares unfavorably to oversampled antiderivative antialiasing. It may therefore be regarded as a negative result, but it may hopefully still form a basis for further developments.

1. INTRODUCTION

Nonlinear systems have become an indispensable part of musical signal processing. In particular, there are many effects such as overdrive, distortion, or other so-called waveshapers, whose primary objective it is to introduce harmonic distortion to enrich the signal.

One major problem encountered when realizing such nonlinear systems digitally is aliasing distortion: Once the additional harmonics introduced by the nonlinearity exceed the Nyquist frequency, they get folded back to lower frequencies, just as if the corresponding analog signal had been sampled without appropriate band-limiting. Contrary to the desired harmonic distortion, aliasing distortion is usually perceived as unpleasant. The conceptually simplest method to reduce aliasing is oversampling. Various alternatives have been proposed that aim to improve the ratio of achieved aliasing suppression to computational cost, e.g. [1, 2, 3, 4].

In this work, we start from an idea similar to [4], namely computing samples not only of the signal after nonlinear distortion, but also of its derivative with respect to time. From the combination of those, perfect reconstruction is possible for signals band-limited to the sampling rate (i.e. twice the original Nyquist limit). Alternatively, signal components between the Nyquist limit and the sampling rate may be suppressed to reduce aliasing when converting to a traditionally sampled signal. By itself, this allows only rather modest aliasing reduction, but as will be shown, it can be very elegantly and beneficially combined with the antiderivative antialiasing of [3].

2. RECONSTRUCTION FROM SAMPLES OF A SIGNAL AND ITS DERIVATIVE

Let $\dot{\bar{x}}(t) = \frac{d}{dt}\bar{x}(t)$ be the derivative with respect to time of a signal $\bar{x}(t)$ and let $x(n) = \bar{x}(nT_\mathrm{s})$ and $\dot{x}(n) = \dot{\bar{x}}(nT_\mathrm{s})$ denote their counterparts when sampled with sampling interval T_s. In [4], such samples are used to determine the coefficients of cubic polynomials and obtain a piecewise cubic signal reconstruction (in that case, of a state trajectory). Here, we instead employ a reconstruction that is more similar to ordinary reconstruction from signal samples, namely of the form

$$\bar{y}(t) = \sum_{n=-\infty}^{\infty} x(n)\hat{h}_1(t - nT_\mathrm{s}) + T_\mathrm{s}\dot{x}(n)\hat{h}_2(t - nT_\mathrm{s}). \quad (1)$$

Note that by omitting the second term, i.e. setting $\hat{h}_2(t) = 0$, and furthermore choosing $\hat{h}_1(t) = \mathrm{sinc}(t)$, this reduces to ordinary reconstruction for signals bandlimited to half the sampling rate. To utilize the derivative's samples, we propose to instead employ

$$\hat{h}_1(t) = (\mathrm{sinc}(t/T_\mathrm{s}))^2 \quad (2)$$

$$\hat{h}_2(t) = \frac{t}{T_\mathrm{s}} \cdot (\mathrm{sinc}(t/T_\mathrm{s}))^2 \quad (3)$$

depicted in figure 1 where

$$\mathrm{sinc}(x) = \begin{cases} \frac{\sin(\pi x)}{\pi x} & \text{for } x \neq 0 \\ 1 & \text{for } x = 0. \end{cases} \quad (4)$$

We first note that

$$\hat{h}_1(nT_\mathrm{s}) = \begin{cases} 1 & \text{for } n = 0 \\ 0 & \text{otherwise} \end{cases} \qquad \frac{d}{dt}\hat{h}_1(t)\Big|_{t=nT_\mathrm{s}} = 0 \quad (5)$$

$$\frac{d}{dt}\hat{h}_2(t)\Big|_{t=nT_\mathrm{s}} = \begin{cases} \frac{1}{T_\mathrm{s}} & \text{for } n = 0 \\ 0 & \text{otherwise} \end{cases} \qquad \hat{h}_2(nT_\mathrm{s}) = 0 \quad (6)$$

so that $\bar{y}(nT_\mathrm{s}) = \bar{x}(nT_\mathrm{s})$ and $\dot{\bar{y}}(nT_\mathrm{s}) = \dot{\bar{x}}(nT_\mathrm{s})$, i.e. the signal and its derivative are reconstructed perfectly at the sampling instants.

To further assess the reconstruction capabilities, we consider the frequency domain, where the frequency responses of the filters as obtained by Fourier transform are given by

$$\hat{H}_1(j\omega) = \begin{cases} T_\mathrm{s} \cdot (1 - \frac{T_\mathrm{s}}{2\pi}|\omega|) & \text{if } |\omega| < \frac{2\pi}{T_\mathrm{s}} \\ 0 & \text{otherwise} \end{cases} \quad (7)$$

$$\hat{H}_2(j\omega) = \begin{cases} \frac{T_\mathrm{s}}{2\pi j}\,\mathrm{sgn}(\omega) & \text{if } |\omega| < \frac{2\pi}{T_\mathrm{s}} \\ 0 & \text{otherwise} \end{cases} \quad (8)$$

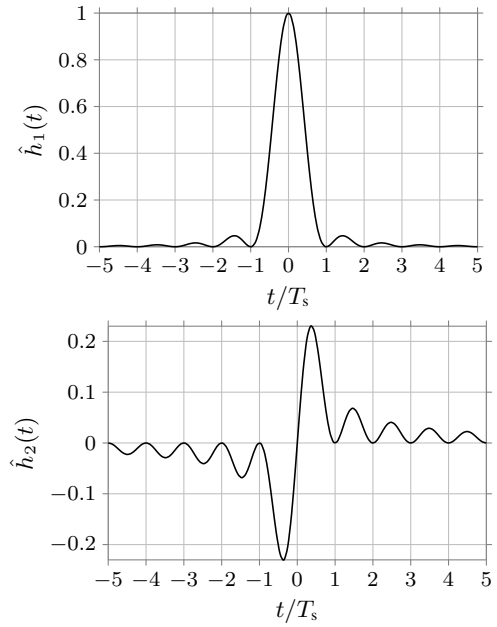

Figure 1: *Reconstruction basis functions*

(see the third row of figure 2). As the reconstruction filters are obviously bandlimited to the sampling frequency $\omega_\mathrm{s} = \frac{2\pi}{T_\mathrm{s}}$, we may at best hope for perfect reconstruction of signals equally bandlimited to ω_s. Now denote the Fourier transform of the input signal $\bar{x}(t)$ as $\bar{X}(j\omega)$. Then the Fourier transform of the sampled signal is given by

$$X(j\omega) = \frac{1}{T_\mathrm{s}} \sum_{k=-\infty}^{\infty} \bar{X}(j(\omega - k\omega_\mathrm{s})) \tag{9}$$

with image spectra appearing at multiples of the sampling frequency. Likewise, with $\dot{\bar{X}}(j\omega) = j\omega\bar{X}(j\omega)$ denoting the Fourier transform of the time derivative $\dot{\bar{x}}(t)$, the Fourier transform after sampling is given by

$$\begin{aligned}\dot{X}(j\omega) &= \frac{1}{T_\mathrm{s}} \sum_{k=-\infty}^{\infty} \dot{\bar{X}}(j(\omega - k\omega_\mathrm{s})) \\ &= \frac{1}{T_\mathrm{s}} \sum_{k=-\infty}^{\infty} j(\omega - k\omega_\mathrm{s})\bar{X}(j(\omega - k\omega_\mathrm{s})).\end{aligned} \tag{10}$$

In the frequency domain, the reconstruction (1) then becomes

$$\begin{aligned}\bar{Y}(j\omega) &= X(j\omega)\hat{H}_1(j\omega) + T_\mathrm{s}\dot{X}(j\omega)\hat{H}_2(j\omega) \\ &= \sum_{k=-\infty}^{\infty} \hat{H}(j\omega; k) \cdot \bar{X}(j(\omega - k\omega_\mathrm{s}))\end{aligned} \tag{11}$$

where

$$\hat{H}(j\omega; k) = \frac{1}{T_\mathrm{s}}\hat{H}_1(j\omega) + j(\omega - k\omega_\mathrm{s})\hat{H}_2(j\omega) \tag{12}$$

can be regarded as the filter effectively applied to the k-th image spectrum. While $\hat{H}(j\omega; k) = 0$ for $|\omega| \geq \omega_\mathrm{s}$ is immediate from the bandlimited nature of $\hat{H}_1(j\omega)$ and $\hat{H}_2(j\omega)$, for $|\omega| < \omega_\mathrm{s}$ we can simplify to

$$\begin{aligned}\hat{H}(j\omega; k) &= (1 - \tfrac{T_\mathrm{s}}{2\pi}|\omega|) + j(\omega - k\omega_\mathrm{s})\tfrac{T_\mathrm{s}}{2\pi j}\operatorname{sgn}(\omega) \\ &= 1 - k\operatorname{sgn}(\omega).\end{aligned} \tag{13}$$

Now let us assume the input signal $\bar{x}(t)$ to be bandlimited to the sampling rate, i.e. such that its Fourier transform obeys $\bar{X}(j\omega) = 0$ for $|\omega| \geq \omega_\mathrm{s}$. Then for $0 < \omega < \omega_\mathrm{s}$, all terms in (11) vanish except for those at $k = 0$ and $k = 1$, as otherwise $|\omega - k\omega_\mathrm{s}| \geq \omega_\mathrm{s}$ and hence $\bar{X}((\omega - k\omega_\mathrm{s})) = 0$. But for $0 < \omega < \omega_\mathrm{s}$, we have $\hat{H}(j\omega; 0) = 1$ and $\hat{H}(j\omega; 1) = 0$, so that (11) reduces to $\bar{Y}(j\omega) = \bar{X}(j\omega)$. Similarly, for $-\omega_\mathrm{s} < \omega < 0$ all terms except for those at $k = 0$ and $k = -1$ vanish, and we have $\hat{H}(j\omega; 0) = 1$ and $\hat{H}(j\omega; -1) = 0$, so that (11) again reduces to $\bar{Y}(j\omega) = \bar{X}(j\omega)$. Thus, for signals bandlimited to the sampling frequency, the method of (1) allows perfect reconstruction.

An example of sampling and reconstruction of a signal bandlimited to ω_s is shown in figure 2 in frequency domain, where the Fourier transform $\bar{X}(j\omega)$ of the original signal (top row left) is assumed real-valued for illustration purposes. The Fourier transform of its derivative is shown on the right. As the signal is not bandlimited to $\frac{\omega_\mathrm{s}}{2}$, the image spectra after sampling, shown in the second row, overlap. But note that (due to the bandlmitation to ω_s) at most two image spectra superimpose at an given frequency. After applying the reconstruction filters shown in the third row, one obtains signals obviously bandlimited to ω_s again, but otherwise not resembling the original signal, see fourth row. However, their weighted sum (bottom) indeed reconstructs the original signal.

2.1. Application to aliasing reduction

To achieve aliasing reduction, instead of reconstructing the original signal, we are interested in obtaining a version of it bandlimited to half the sampling rate, or rather samples thereof. Bandlimiting the frequency responses from (7) and (8) to $\frac{\omega_\mathrm{s}}{2} = \frac{\pi}{T_\mathrm{s}}$ then trivially results in

$$\bar{H}_1(j\omega) = \begin{cases} T_\mathrm{s} \cdot (1 - \frac{T_\mathrm{s}}{2\pi}|\omega|) & \text{if } |\omega| < \frac{\pi}{T_\mathrm{s}} \\ 0 & \text{otherwise} \end{cases} \tag{14}$$

$$\bar{H}_2(j\omega) = \begin{cases} \frac{T_\mathrm{s}}{2\pi j}\operatorname{sgn}(\omega) & \text{if } |\omega| < \frac{\pi}{T_\mathrm{s}} \\ 0 & \text{otherwise} \end{cases} \tag{15}$$

with the corresponding impulse responses

$$\bar{h}_1(t) = \frac{1}{2}\operatorname{sinc}(t/T_\mathrm{s}) + \frac{1}{4}\left(\operatorname{sinc}(t/2T_\mathrm{s})\right)^2 \tag{16}$$

$$\bar{h}_2(t) = \frac{t}{4T_\mathrm{s}} \cdot \left(\operatorname{sinc}(t/2T_\mathrm{s})\right)^2 \tag{17}$$

derived via inverse Fourier transform. Reconstructing with $\bar{H}_1(j\omega)$ and $\bar{H}_2(j\omega)$ instead of $\hat{H}_1(j\omega)$ and $\hat{H}_2(j\omega)$, we have to replace $\hat{H}(j\omega_0; k)$ in (11) with

$$\bar{H}(j\omega; k) = \begin{cases} \hat{H}(j\omega; k) & \text{for } |\omega| < \frac{\omega_\mathrm{s}}{2} \\ 0 & \text{otherwise,} \end{cases} \tag{18}$$

likewise bandlimited to $\frac{\omega_\mathrm{s}}{2}$.

We assess the effectiveness for antialiasing by assuming a complex exponential $\bar{x}(t) = e^{j\omega_0 t}$ as original signal with the

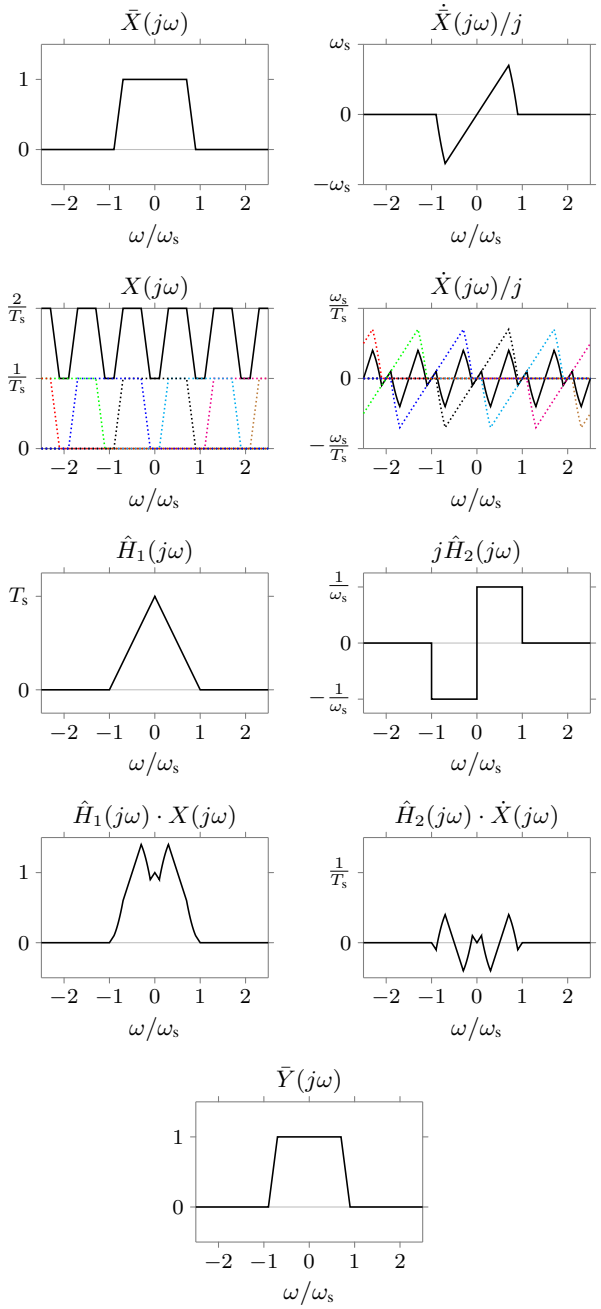

Figure 2: *Example of sampling and reconstruction of a signal bandlimited to ω_s, frequency domain representation. Top row: example signal (assuming a real-valued Fourier transform for illustration) and its derivative. Second row: the same signals after sampling, colorful dotted lines indicate individual image spectra, solid line their superposition. Third row: the two reconstruction filters. Fourth row: signals after application of the respective reconstruction filters. Bottom: the reconstructed signal.*

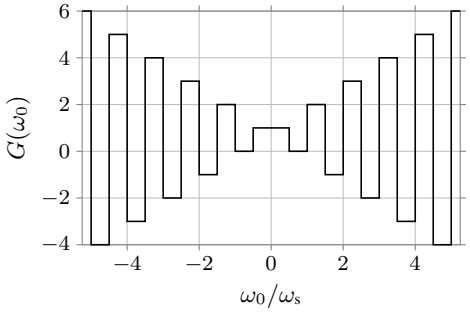

Figure 3: *Input-frequency-dependent gain $G(\omega_0)$ of signals sampled and reconstructed with $\bar{H}_1(j\omega)$ and $\bar{H}_2(j\omega)$*

corresponding Fourier transform $\bar{X}(j\omega) = \delta(\omega - \omega_0)$ given by a single Dirac impulse at ω_0 potentially exceeding the sampling rate. Sampling and reconstruction (bandlimited to $\frac{\omega_\mathrm{s}}{2}$) then gives

$$\begin{aligned}\bar{Y}(j\omega) &= \sum_{k=-\infty}^{\infty} \bar{H}(j\omega; k) \cdot \delta(\omega - \omega_0 - k\omega_\mathrm{s}) \\ &= \sum_{k=-\infty}^{\infty} \bar{H}(j(\omega_0 + k\omega_\mathrm{s}); k) \cdot \delta(\omega - \omega_0 - k\omega_\mathrm{s}). \end{aligned} \tag{19}$$

Here, all terms vanish where $|\omega_0 + k\omega_\mathrm{s}| \geq \frac{\omega_\mathrm{s}}{2}$ due to the bandlimitedness of $\bar{H}(j\omega; k)$, leaving only a single term at $k_0 = -\left[\frac{\omega_0}{\omega_\mathrm{s}}\right]$ (with $[\cdot]$ denoting rounding to the nearest integer). We thus arrive at

$$\bar{Y}(j\omega) = \bar{H}(j(\omega_0 + k_0\omega_\mathrm{s}); k_0) \cdot \delta(\omega - \omega_0 - k_0\omega_\mathrm{s}) \tag{20}$$

or equivalently

$$\bar{y}(t) = \bar{H}(j(\omega_0 + k_0\omega_\mathrm{s}); k_0) \cdot e^{j(\omega_0 + k_0\omega_\mathrm{s})t}. \tag{21}$$

So all in all, the complex exponential is aliased to the baseband and weighted with

$$G(\omega_0) = \hat{H}(j(\omega_0 + k_0\omega_\mathrm{s}); k_0) = 1 + \left[\frac{\omega_0}{\omega_\mathrm{s}}\right] \cdot \operatorname{sgn}\left(\frac{\omega_0}{\omega_\mathrm{s}} - \left[\frac{\omega_0}{\omega_\mathrm{s}}\right]\right) \tag{22}$$

as depicted in figure 3. We observe that $G(\omega_0) = 1$ for $|\omega_0| < \omega_\mathrm{s}/2$, confirming perfect reconstruction up to half the sampling rate, and $G(\omega_0) = 0$ for $\omega_\mathrm{s}/2 < |\omega_0| < \omega_\mathrm{s}$, perfect suppression of aliased components up to the sampling rate. However, for signals with even higher frequency, the aliased components are actually amplified, owing to the high-frequency gain of the involved differentiation.

For signals with components exceeding half the sampling rate but then decaying quickly with frequency, the approach may nevertheless result in a net benefit. However, to be practical, it has to be applied in the discrete-time domain to obtain signals of an antialiased signal that can then be processed like any other signal. As $\bar{h}_1(t)$ and $\bar{h}_2(t)$ are by construction sufficiently band-limited, they can be safely sampled and the reconstruction be replaced with a convolution. Following this approach, we obtain

$$h_1(n) = \bar{h}_1(nT_\mathrm{s}) = \frac{1}{2}\operatorname{sinc}(n) + \frac{1}{4}\left(\operatorname{sinc}(n/2)\right)^2 \tag{23}$$

$$h_2(n) = \bar{h}_2(nT_\mathrm{s}) = \frac{1}{4}n \cdot \left(\operatorname{sinc}(n/2)\right)^2 \tag{24}$$

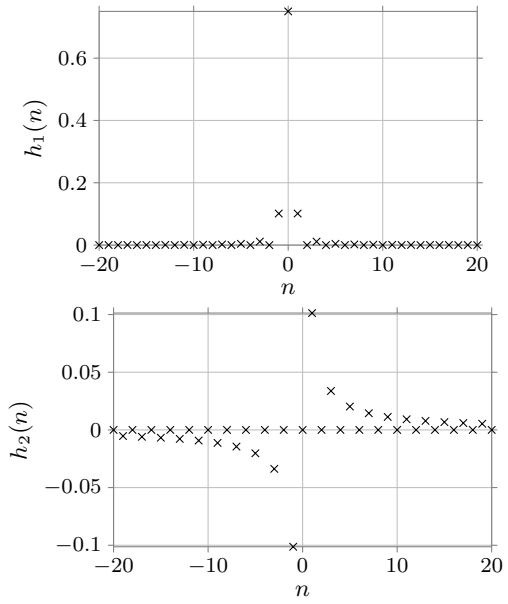

Figure 4: *Sampled bandlimited reconstruction basis functions*

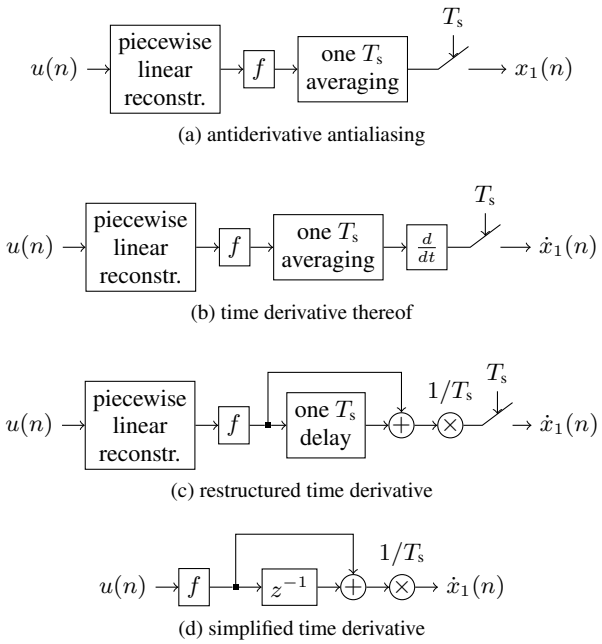

Figure 5: *Equivalent system representation of antiderivative antialiasing and its time derivative*

as depicted in figure 4 and the antialiasing operation

$$y(n) = \sum_{k=-\infty}^{\infty} h_1(k)x(n-k) + h_2(k)T_s\dot{x}(n-k). \tag{25}$$

3. COMBINATION WITH ANTIDERIVATIVE ANTIALIASING

As the origin of signals with aliased components, we consider nonlinear mappings of the form

$$\bar{x}(t) = f(\bar{u}(t)) \tag{26}$$

where $\bar{u}(t)$ is bandlimited to $f_s/2$ but $\bar{x}(t)$ generally is not due to the emergence of harmonics. Thus, the discrete-time operation $x(n) = f(u(n))$ suffers from aliasing distortion. To try and reduce aliasing by utilizing the time derivative as explained above, we require

$$\dot{\bar{x}}(t) = \frac{d}{dt} f(\bar{u}(t)) = \dot{\bar{u}}(t) f'(\bar{u}(t)) \tag{27}$$

where $f'(\bar{u}) = \frac{d}{d\bar{u}} f(\bar{u})$. It is thus easy to obtain samples $\dot{x}(n) = \dot{u}(n)f'(u(n))$ if given $\dot{u}(n)$, which could be obtained from $u(n)$ with appropriate linear filters. In the light of the discussion in section 2, this scheme could be applied if $f(u)$ is sufficiently mild so that the introduced harmonics roll off quickly.

To make the approach also applicable to more aggressive $f(u)$, we propose to first replace it with a version that ensures sufficient high-frequency roll-off by employing antiderivative antialiasing [3]. It consists of (virtually) reconstructing a continuous-time signal, applying the nonlinearity to it, lowpass filtering, and sampling to obtain a discrete-time signal again. To make this approach computable, the reconstruction uses simple linear interpolation and the lowpass will also be kept relatively simple. In the first-order case, it only performs averaging over one sampling interval, resulting in the system of figure 5a. Its output is given by

$$x_1(n) = \int_0^1 f(\tilde{u}(\tau; n))d\tau \tag{28}$$

with

$$\tilde{u}(\tau; n) = (1-\tau)\cdot u(n-1) + \tau \cdot u(n). \tag{29}$$

Observing $\frac{d\tilde{u}}{d\tau} = u(n) - u(n-1)$, we can now perform integration by substitution to obtain

$$x_1(n) = \frac{\int_{u(n-1)}^{u(n)} f(\tilde{u})d\tilde{u}}{u(n) - u(n-1)}. \tag{30}$$

Applying the fundamental theorem of calculus and with continuos extension for $u(n) = u(n-1)$ by taking the limit in that case, we finally arrive at

$$x_1(n) = \begin{cases} \frac{F(u(n)) - F(u(n-1))}{u(n) - u(n-1)} & \text{if } u(n) \neq u(n-1) \\ \frac{1}{2}(f(u(n)) + f(u(n-1))) & \text{if } u(n) = u(n-1) \end{cases} \tag{31}$$

where $F(u)$ denotes the antiderivative of $f(u)$.

To obtain samples $\dot{x}_1(n)$ of the derivative corresponding to the output of this modified nonlinearity, we start by adding a differentiation to the system of figure 5a, yielding the system of figure 5b. But averaging and differentiating are both linear filtering operations that can be combined into a single linear filter. In particular, averaging over one sampling period is equivalent to convolution with

$$g_1(t) = \begin{cases} \frac{1}{T_s} & \text{for } 0 \leq t \leq T_s \\ 0 & \text{otherwise,} \end{cases} \tag{32}$$

the derivative of which is given by

$$\frac{d}{dt} g_1(t) = \frac{1}{T_s}\left(\delta(t) - \delta(t - T_s)\right) \tag{33}$$

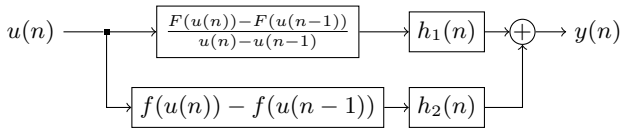

Figure 6: *Combined derivative/antiderivative antialiasing system*

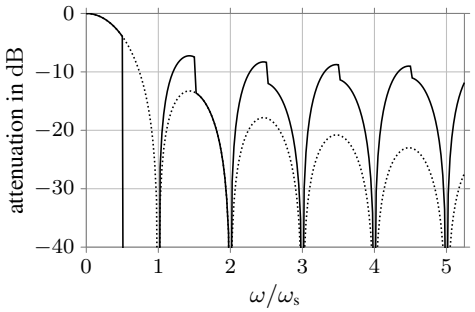

Figure 7: *Attenuation of signal components by antiderivative antialiasing alone (dotted) and in combination with the derivative-based approach (solid)*

where $\delta(t)$ denotes the Dirac delta distribution. This leads to the system of figure 5c. Now observe that we only need to evaluate the output of the nonlinearity at sampling instants. And with the nonlinearity being stateless, the same holds for its input, i.e. the output of the piecewise linear reconstruction. But at the sampling instants, its output is equal to its input, so that the whole operation reduces to

$$\dot{x}_1(n) = \frac{1}{T_s}(f(u(n)) - f(u(n-1))) \tag{34}$$

depicted in figure 5d. It should be emphasized that while this is the first-order differences approximation of the time-derivative of the original system, it is the exact time-derivative of the antiderivative-antialiased system.

As one might have hoped for, derivative and antiderivative cancel and we are left with an astonishingly simple result. In particular, note that we no longer require $\dot{u}(n)$, eliminating the need for a linear filter to estimate it. Noting that the factors T_s and $\frac{1}{T_s}$ from (25) and (34) cancel, we finally arrive at the combined system depicted in figure 6.

The averaging operation of the antiderivative antialiasing corresponds to a sinc-shaped frequency response, attenuating high-frequency components before they are aliased into the baseband. In combination with the derivative-based approach, it combines with the transfer characteristic of figure 3, resulting in the frequency response shown in figure 7 (solid line). The comparison with the responses of antiderivative antialiasing alone (dotted) verifies that the strongest unwanted components just above $\omega_s/2$ are completely removed, at the cost of reduced attenuation of higher-frequency components.

Another interesting comparison concerns the effect when the antialiasing approaches are (unnecessarily) applied to a linear $f(u)$. In particular, we consider $f(u) = u$. In that case, first-oder antiderivative antialiasing leads to $x_1(n) = \frac{1}{2}(u(n) + u(n-1))$,

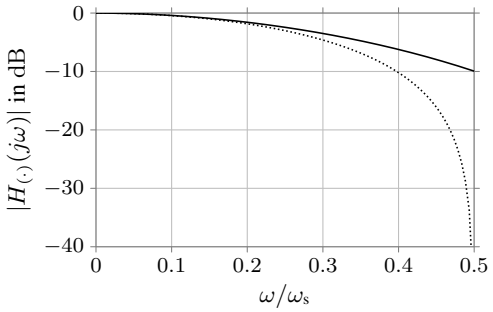

Figure 8: *Frequency response of antiderivative antialiasing (dotted) and the combined approach (solid) when applied to the identity function $f(u) = u$*

while the combination with the derivative leads to

$$\begin{aligned} y(n) &= \sum_{k=-\infty}^{\infty} \frac{1}{2} h_1(k)(x_1(n-k) + x_1(n-k-1)) \\ &\qquad + h_2(k)(x_1(n-k) - x_1(n-k-1)) \\ &= \sum_{k=-\infty}^{\infty} \left(\tfrac{1}{2}(h_1(k) + h_1(k-1)) + h_2(k) - h_2(k-1)\right) \\ &\qquad \cdot x_1(n-k). \end{aligned} \tag{35}$$

The corresponding frequency responses are given by

$$H_a(j\omega) = \cos(\omega T_s/2) e^{j\omega T_s/2} \tag{36}$$

for antiderivative antialiasing and

$$H_c(j\omega) = \left(\cos(\tfrac{\omega T_s}{2})\bar{H}_1(j\omega) + 2\sin(\tfrac{\omega T_s}{2})\bar{H}_2(j\omega)\right) e^{j\omega T_s/2} \tag{37}$$

for the combined approach (for $|\omega| < \omega_s$). As can be seen in figure 8, the combined approach has significantly lower high-frequency loss when applied to a linear function. The same behavior may be expected when a nonlinear function is used but excited with a small signal, mainly operating in the linear region. It should be noted, though, that these frequency responses only affect the fundamental in the (almost) linear case. Harmonics appearing in the nonlinear case are always primarily subject to the sinc-shaped frequency response of the one-T_s-averaging, for both the antiderivative and the combined antialiasing approach alike.

3.1. Second-order antiderivative antialiasing

Different extensions of antiderivative antialiasing to higher orders have been proposed [5, 6]. Here, we will only consider the approach of [3] in which the rectangular filter kernel corresponding to an averaging over one sampling period is replaced with a triangular one

$$g_2(t) = \begin{cases} \frac{1}{T_s} \cdot \frac{t}{T_s} & \text{for } 0 < t \le T_s \\ \frac{1}{T_s}\left(2 - \frac{t}{T_s}\right) & \text{for } T_s < t \le 2T_s \\ 0 & \text{otherwise.} \end{cases} \tag{38}$$

This leads to

$$x_2(n) = \frac{u(n)\cdot(F(u(n)) - F(u(n-1)))}{(u(n)-u(n-1))^2} - \frac{F_1(u(n)) - F_1(u(n-1))}{(u(n)-u(n-1))^2} + \frac{u(n-2)\cdot(F(u(n-2)) - F(u(n-1)))}{(u(n-2)-u(n-1))^2} - \frac{F_1(u(n-2)) - F_1(u(n-1))}{(u(n-2)-u(n-1))^2} \quad (39)$$

where $F_1(u) = \int u f(u) du$ (with special cases when the denominators vanish, see [3]).

Like for the first-order case, we can obtain the derivative by differentiating $g_2(t)$, giving

$$\frac{d}{dt} g_2(t) = \begin{cases} \frac{1}{T_\mathrm{s}^2} & \text{for } 0 < t \le T_\mathrm{s} \\ -\frac{1}{T_\mathrm{s}^2} & \text{for } T_\mathrm{s} < t \le 2T_\mathrm{s} \\ 0 & \text{otherwise} \end{cases} \quad (40)$$
$$= \frac{1}{T_\mathrm{s}} \left(g_1(t) - g_1(t - T_\mathrm{s}) \right).$$

Noting that convolution with $g_1(t)$ brings us back to the first-oder case, we thus arrive at

$$\dot{x}_2(n) = \frac{1}{T_\mathrm{s}} \left(x_1(n) - x_1(n-1) \right). \quad (41)$$

4. EVALUATION

To evaluate the effectiveness of the proposed method, we consider the soft-clipping nonlinearity given by

$$f(u) = \frac{2}{\pi} \arctan(u). \quad (42)$$

The antiderivatives required for antiderivative antialiasing are

$$F(u) = \frac{2}{\pi} \left(u \arctan(u) - \tfrac{1}{2} \log(1 + u^2) \right) \quad (43)$$

$$F_1(u) = \frac{1}{\pi} \left((u^2 + 1) \arctan(u) - u \right). \quad (44)$$

To obtain an implementable system for the derivate-based antialiasing, we truncate the filter impulse responses $h_1(n)$ and $h_2(n)$. Thanks to its fast decay, we can truncate $h_1(n)$ to $-7 \le n \le 7$. As $h_2(n)$ decays slower, we choose a much longer excerpt, namely $-99 \le n \le 99$ and multiply with a Hann window $w(n) = \cos^2(\frac{\pi}{198} n)$. More careful filter design may be able to reduce the filter order even further without compromising quality. But even with the given design, as every second coefficient of the filter impulse responses is zero and by exploiting their symmetry, the filters can be computed with a total of 54 multiplications per sample, showing the practical feasibility.

The system is excited with a single sinusoid

$$u(n) = 10 \sin(2\pi f_0 T_\mathrm{s} n) \quad (45)$$

at a frequency of $f_0 = 1318.5\,\mathrm{Hz}$ and sampling rate $1/T_\mathrm{s} = 44.1\,\mathrm{kHz}$. Figure 9 shows the resulting spectrum of the output without antialiasing. Strong aliasing distortion is clearly visible.

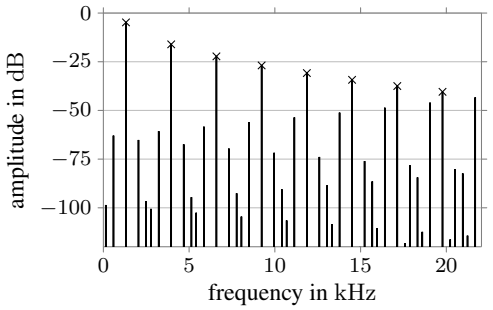

Figure 9: *Output spectrum without antialiasing. Crosses mark desired harmonics.*

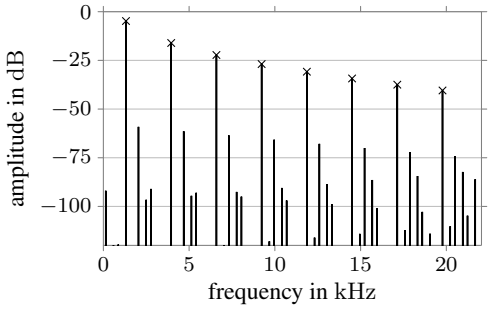

Figure 10: *Output spectrum when using derivative-based antialiasing. Crosses mark desired harmonics.*

For this particular input, we can determine samples of the output's derivative as

$$\dot{x}(n) = \frac{40 f_0 \cos(2\pi f_0 T_\mathrm{s} n)}{1 + (10 \sin(2\pi f_0 T_\mathrm{s} n))^2}. \quad (46)$$

Figure 10 confirms that applying derivative-based antialiasing according to (25) suppresses the strongest aliasing components. However, closer inspection reveals that the remaining aliasing sees a slight increase. Overall, the aliasing has been reduced, but not to a satisfactory level.

As can be seen in figure 11a, first-order antiderivative antialiasing has the opposite effect: it greatly reduces overall aliasing, but does little to the strongest aliasing components primarily at higher frequencies. When combined with the derivative-based approach, figure 11b shows that these most prominent aliasing components are dramatically attenuated, at the cost of a slight increase of the remaining aliasing. Finally, in figure 11c we compare with antiderivative antialiasing oversampled by a factor of two, which exhibits even better aliasing suppression. For simplicty and comparability, the interpolation and decimation filters for the sampling rate conversion are Hann-windowed sinc functions of the same length as h_1 for the interpolation and as h_2 for the decimation filter, respectively. With a more sophisticated decimation filter design, further suppression of the strong aliasing component at $21.7\,\mathrm{kHz}$ could certainly be achieved, which should however be imperceptible anyway.

The same comparison is carried out in figure 12 for second-order antiderivative antialiasing. As expected, it performs better than first-order antiderivative antialiasing, but on its own, it leaves some strong aliasing components especially at higher frequencies, see figure 12a. Again, combination with derivate-based antialiasing

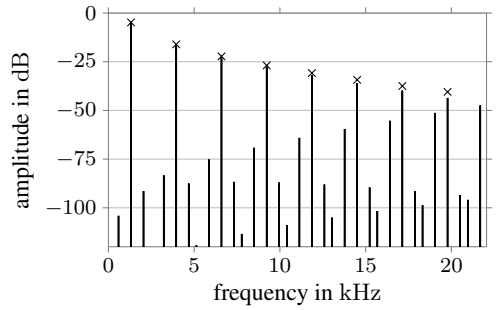

(a) first-order antiderivative antialiasing

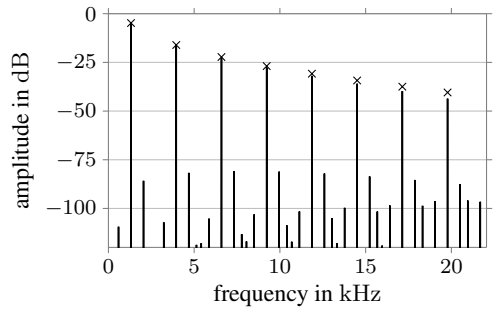

(b) combined derivative/first-order antiderivative antialiasing

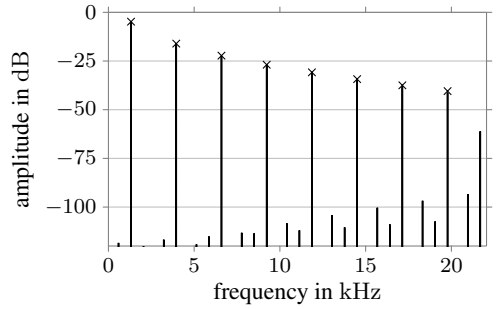

(c) two times oversampled first-order antiderivative antialiasing

Figure 11: *Comparison of first-order antiderivative antialiasing with and without combination with derivative-based antialiasing or oversampling by a factor of two. Crosses mark desired harmonics.*

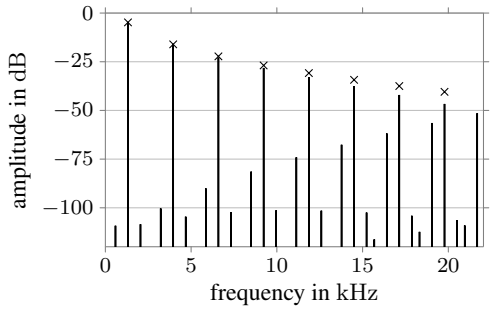

(a) second-order antiderivative antialiasing

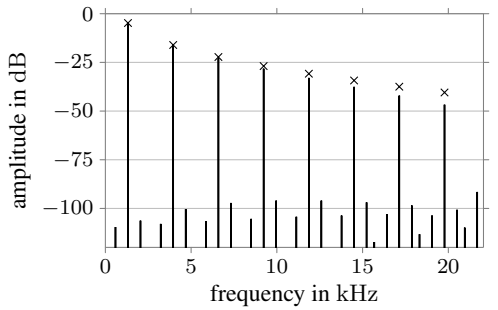

(b) combined derivative/second-order antiderivative antialiasing

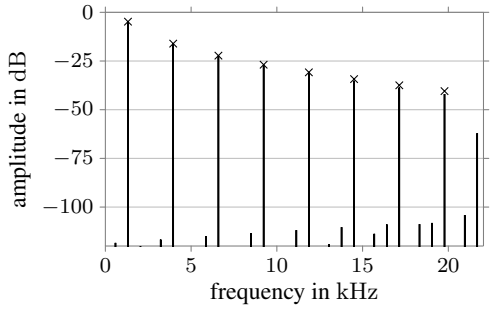

(c) two times oversampled second-order antiderivative antialiasing

Figure 12: *Comparison of second-order antiderivative antialiasing with and without combination with derivative-based antialiasing or oversampling by a factor of two. Crosses mark desired harmonics.*

reduces these but slightly increases the remaining aliasing as shown in figure 12b. Finally, figure 12c confirms that also for the second-order case, oversampling by a factor of two is even more effective.

5. DISCUSSION

The derivative-based antialiasing developed in section 2 nicely complements antiderivative antialiasing: They reduce each other's weaknesses while only mildly affecting their strengths. At the same time, the derivative and antiderivative computation cancel to a large extent, resulting in a relatively simple system. However, combining antiderivative antialiasing with oversampling by a factor of two is also conceptually simple and even more effective at aliasing suppression.

That raises the question which one is more efficient. If the combined approach is computationally more efficient than two times oversampled antiderivative antialiasing, it could be an interesting alternative. However, an exact answer will involve a lot of "it depends", so we only do a qualitative discussion here. Ignoring the $u(n) = u(n-1)$ case for simplicity, every evaluation of (31) requires one evaluation of $F(u(n))$ (assuming $F(u(n-1))$ has been stored from the previous time step) and one division. Two-times oversampling obviously doubles that. Combination with derivative-based antialiasing instead requires an additional evaluation of $f(u(n))$. The difference in computational complexity between these two will probably not be significant but tend to favour the derivative-based approach. For second-order antiderivative antialiasing, combination with the derivative-based approach

has a clearer advantage over oversampling by a factor of two, as $x_1(n)$ given by (31) can be found as a subexpression in (39), so that additionally computing the derivative with (41) is almost free, while oversampling will require additional evaluations of F and F_1 and divisions.

In addition to the nonlinear part, both the derivative-based approach and oversampling require linear filtering. The exact filter order and, after exploiting zero-coefficients and symmetry, number of multiplications depends on the filter design used. But both approaches have in common that they require one long filter (h_2 for the derivative-based approach, the decimation filter for oversampling) and one short filter (h_1 for the derivative-based approach, the interpolation filter for oversampling, considering [7]). If the evaluation of the nonlinear functions is relatively cheap and the computational complexity is therefore dominated by the linear filtering, it is roughly comparable for both approaches.

To conclude, the combined derivative/antiderivative antialiasing developed in this paper may be conceptually elegant, but it offers no real benefit compared to two-times oversampled antiderivative antialiasing. On the contrary, it is less effective while any advantages in terms of computational complexity may likely be insignificant. We nevertheless hope to stimulate further research in this area, maybe leading to further developments that then do offer actual benefits.

6. REFERENCES

[1] Fabián Esqueda and Vesa Välimäki, "Rounding corners with BLAMP," in *Proc. 19th Int. Conf. on Digital Audio Effects (DAFx-16)*, Brno, Czech Republic, 2016, pp. 121–128.

[2] Fabián Esqueda, Vesa Välimäki, and Stefan Bilbao, "Antialiased soft clipping using an integrated bandlimited ramp," in *Proc. 24th European Signal Process. Conf. (EUSIPCO)*, Budapest, Hungary, 2016, pp. 1043–1047.

[3] Julian D. Parker, Vadim Zavalishin, and Efflam Le Bivic, "Reducing the aliasing of nonlinear waveshaping using continuous-time convolution," in *Proc. 19th Int. Conf. on Digital Audio Effects (DAFx-16)*, Brno, Czech Republic, 2016, pp. 137–144.

[4] Rémy Muller and Thomas Hélie, "Trajectory anti-aliasing on guaranteed-passive simulation of nonlinear physical ssystems," in *Proc. 20th Int. Conf. on Digital Audio Effects (DAFx-17)*, Edinburgh, UK, 2017, pp. 87–94.

[5] Stefan Bilbao, Fabián Esqueda, Julian D. Parker, and Vesa Välimäki, "Antiderivative antialiasing for memoryless nonlinearities," *IEEE Signal Process. Lett.*, vol. 24, no. 7, pp. 1049–1053, 2017.

[6] Stefan Bilbao, Fabian Esqueda, and Vesa Välimäki, "Antiderivative antialiasing, lagrange interpolation and spectral flatness," in *Proc. IEEE Workshop on Appl. of Signal Process. to Audio and Acoust. (WASPAA)*, New Paltz, NY, USA, 2017, pp. 141–145.

[7] Julen Kahles, Fabián Esqueda, and Vesa Välimäki, "Oversampling for nonlinear waveshaping: Choosing the right filters," *J. Audio Eng. Soc.*, vol. 67, no. 6, pp. 440–449, 2019.